Final-Reporting-2

Title of research:

Behaviour and Design of Composite Metal Deck Diaphragms Subjected to In-plane Shear Forces

PhD student:

Hooman Rezaeian

The University of Auckland

Supervisors:

Associate Professor Charles Clifton

Associate Professor James Lim

May 2019

Abstract

During an earthquake, the floors of a multistorey building are designed to function as rigid in-plane diaphragms. As such they are subjected to significant shear demand, especially at the interfaces between each floor and the seismic resisting system. They have to remain elastic to be a rigid diaphragm. However, the behaviour of composite floor slab diaphragm interfaces in the elastic and the inelastic range has not been previously researched, so designers are forced to be very conservative when determining the limits for elastic behaviour the different failure modes of composite floors subjected to in-plane shear forces have been determined by a number of researchers using pseudo-static testing. However, all previous experimental tests subjected the floors to a combination of shear and moment and did not represent the boundary conditions applying at the diaphragm interfaces with the seismic resisting system. This paper proposes a new experimental test setup in which the slabs being tested are subjected to near pure shear at the slab to supporting beam interface. Using the new experimental test setup, three composite floor slabs comprising a reinforced concrete slab on trapezoidal steel deck have been tested. In the first floor slab, the deck rib orientation is parallel to the supporting beam. For second and third floor slab configuration, the deck rib orientation is perpendicular to the supporting beam. The second floor slab uses the standard end anchorage details adopted in New Zealand, involving a solid rib of concrete surrounding the shear studs along the secondary beam. The third floor slab uses the standard end anchorage detail adopted in Europe, in which the decking runs a short distance over the secondary beam and the shear studs are welded through the decking.

It was found that all three slabs had similar strength and stiffness, albeit with different failure modes. The first slab exhibited the most brittle behaviour, with a sharp drop in load carrying capacity following attainment of peak load. The second and third slabs showed a more stable behaviour, with the New Zealand end anchorage details exhibiting a smoother post-peak behaviour and being the most ductile detail among these three end anchorage details. A comparison between the test results and existing design diaphragm interface shear capacity design equations has been made and a new equation is developed to better represent the in plane shear strength of composite floor slab diaphragms.

Nomenclature

A_{rt}	Area of transverse reinforcement crossing shear planes
b	Depth of the slab (See Fig. 7)
Δ_p	Displacement at ultimate shear strength
E_d	Energy dissipation
f_{yr}	Yield stress of tension reinforcement in the composite slab
$f_c{}'$	Specified concrete cylinder compression strength at 28 days
K_e	Elastic shear stiffness
$K_{1.5y_d}$	Stiffness at $1.5y_d$
n_s	Shear modulus ratio of steel deck to concrete
p	Pitch of one rib (See Fig. 3)
p'	Developed width of one flute
t	Thickness of steel deck
t_c	Average thickness of slab
t_e	Effective thickness of slab
V_r	Ultimate shear strength
$V_{r,exp}$	V_r measured experimentally
y_d	Corresponding displacement to yielding point

List of Tables

List of Figures

1 Introduction

Composite steel deck concrete floor systems (see Fig. 1), referred to as composite slabs, are used widely in steel framed multi-storey buildings [1, 2]. Apart from resisting gravity load, composite slabs also distribute lateral loads to the lateral load resisting system by acting as rigid diaphragms. This rigid behaviour is assumed when determining the transfer of load between the composite slab and the lateral load resisting system, therefore it is important that elastic behaviour occurs in practice, otherwise the load transfer mechanism will not be the same as that assumed in design, leading to potentially poor behaviour.

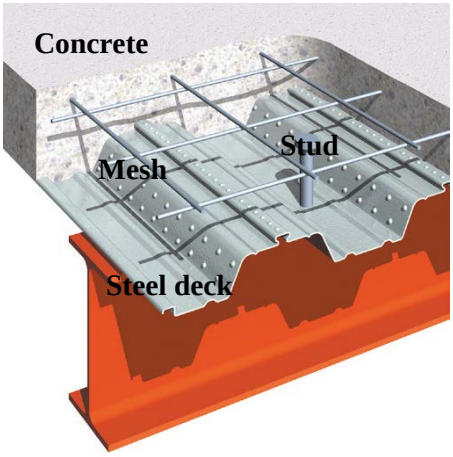

Figure 1. Composite slab section

In New Zealand, inelastic response of diaphragms designed to be elastic was observed in many reinforced concrete buildings in the Canterbury earthquake series of 2010 and 2011. In some instances, this was sufficiently severe to result in the demolition of these buildings, even though the seismic resisting systems performed well. The same behaviour was observed following the Kaikoura earthquake of November 2016 in Wellington, where a number of reinforced concrete buildings constructed after 1970, needed to be either demolished or have major repairs. In the case of the steel structures, the composite slab diaphragms exhibited cracks and damage, mostly across the edge zone where the diaphragm in plane forces transfer to the seismic resisting system (see Fig. 2). There was some uncertainty about their residual seismic capacities.

Thus, observations from recent earthquakes in New Zealand has demonstrated that diaphragms can exhibit poor behaviour during a severe earthquake when the demands are larger than those predicted by the design codes, which is common in a severe earthquake. Recent

Figure 2. Pacific tower floor cracks after Christchurch earthquake 2011

shake table tests has also shown the same poor behaviour [3, 4]. Consequently, research on characterizing the elastic, inelastic, post-peak behaviour and energy dissipation of diaphragms is urgently required.

In the literature, many studies have investigated the flexural behaviour of composite steel deck floors, for example, Easterling and Young 1992 [5], Abdullah and Easterling 2007 [6], Lopes and Simoes 2008 [7], Hedaoo et al. 2012 [8]. Very few studies have considered the in-plane shear behaviour.

Recently, Altoubat et al. [9] studied the in-plane shear behaviour of composite floors, with the focus of the work was on the effect of the steel fibre reinforcement. Prior to this, the last major studies considering in-plane shear behaviour of composite slabs were in the 1970s by Luttrell and Winter [10] and in the 1980s by Davies and Fisher [11], Easterling [12] and Porter and Greimann [13]. It should be noted that almost all the aforementioned tests were under monotonic loading, with only Easterling [12] considering cyclic tests. It should also be noted that the test-rig used in all these previous experimental rests resulted in a combination of shear and moment, as shown conceptually in Fig. 3a.

This paper presents results from a test setup, as shown conceptually in Fig. 3b, in which the slab is under pure shear. This is achieved by preventing the slab from twisting. Using the proposed test setup, three composite floor slabs have been tested, each slab having overall dimensions are of 1.7 m x 1.16 m x 0.125 m. Fig. 4 shows the geometric dimensions of steel decking used to manufacture composite slabs. In the first composite slab, the rib orientation is parallel to the supporting beam. For second and third floor slabs, perpendicular to the supporting

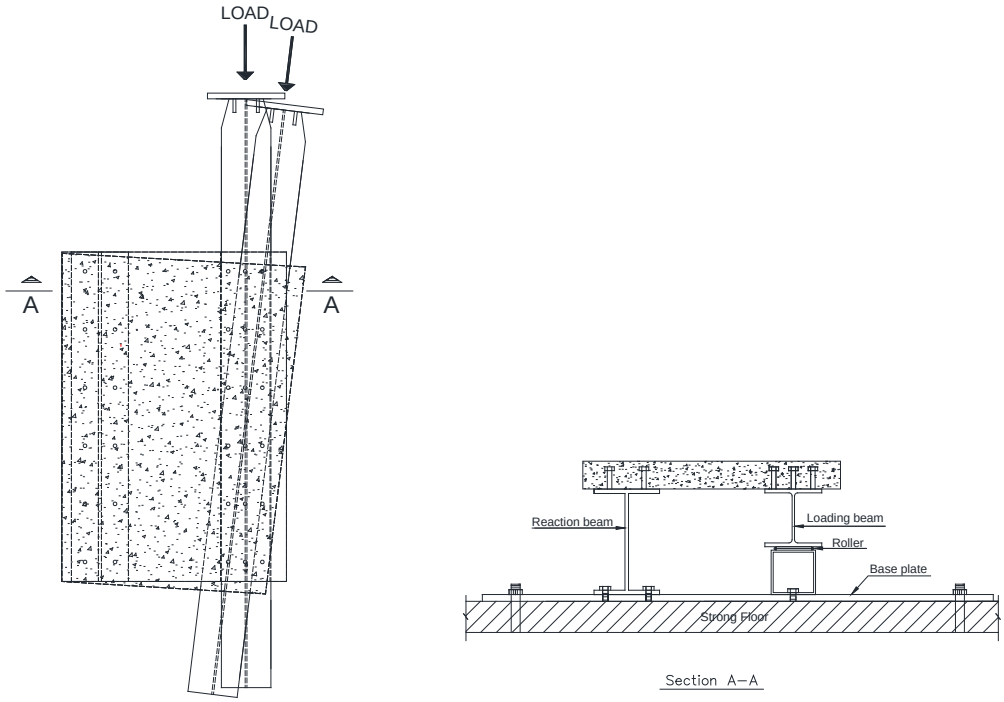

a) Conventional test setup

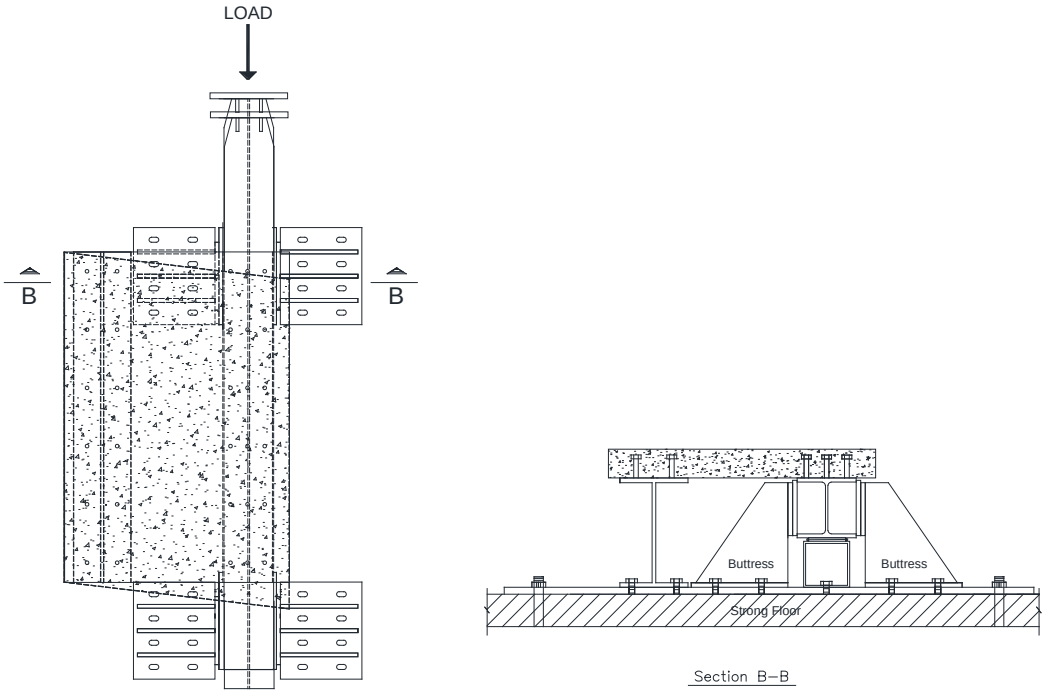

b) Proposed test setup

Figure 3. Schematic forces generated in specimen by test rigs

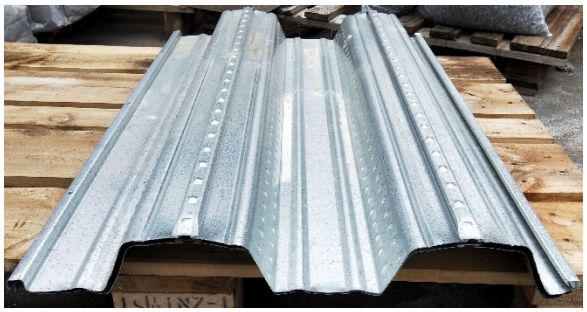

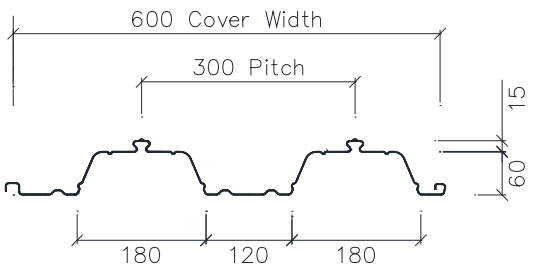

a) Photograph of steel deck b) Dimensions of steel deck

Figure 4. Steel deck configuration

beam, standard New Zealand and standard European / North American end anchorage details were adopted (see Fig. 5). Three specimens of each type were tested; the first monotonically and the second and third cyclically. All three specimens had a quite similar strength and stiffness. Specimen 2 demonstrated the most ductile behaviour with a stable and smooth post peak behaviour among three specimens while specimen 1 presented a brittle behaviour with a significant fall in the post-peak strength as described in this paper.

A comparison between the test results and codified equations (EN 1994-1-1:2004, AS/NZS 2327:2017 and NZ 3404) has been made and a new equation has been developed to determine in plane shear strength of composite diaphragms.

(a) Sp2: New Zealand detail (b) Sp3: European detail

Figure 5. End anchorage detail perpendicular to the beam

2 Experimental program

2.1 Test setup description

Fig. 6 shows a schematic of the test rig to assess the in-plane shear behaviour of composite slabs. As mentioned before, the specimen twisting was prevented by buttresses. These tests were conducted in the structures testing laboratory at The University of Auckland.

As can be seen from Fig. 6, the composite slab under consideration was supported by a reaction beam and a loading beam. The reaction beam was a 475PB147 steel section of length 1.7m. The loading beam was a 250UC89.5 section of length 2.9 m; it was seated on 16 mm diameter steel rollers and could move on a support beam of length 1.9 m, which was a 200x2009HS steel section to provide the conditions of in-plane movement.

The bottom flange of the reaction beam was attached to the 2350x2300x32 base plate through a set of 16 high strength M24 screws and the base plate was anchored to the strong floor by post-tensioning 40mm diameter high strength steel rods.

To prevent the loading beam from twisting due to the complementary shear forces, four buttresses were constructed and placed on both sides of the loading beam to apply shear force. Each buttress was screwed to the base plate using 8 high-strength M24 screws. To reduce friction between the loading beam and the buttresses, PTFE sheets were used. A 1000 kN MTS actuator was employed to apply in-plane shear force with a rate of 0.01mm/s until failure occurred.

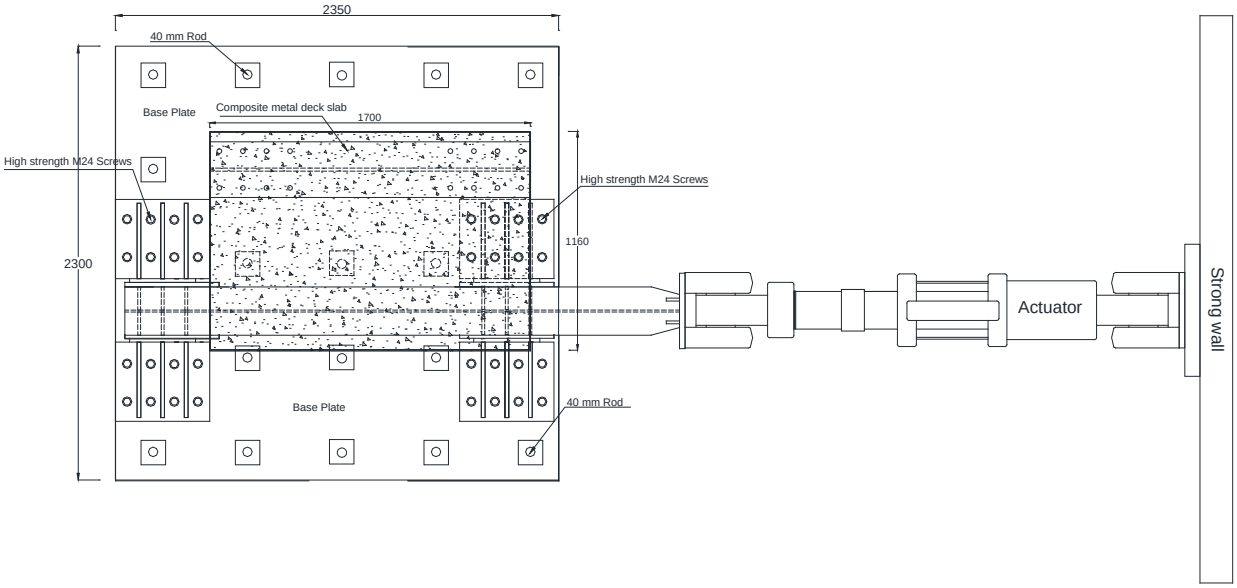

a) Top view

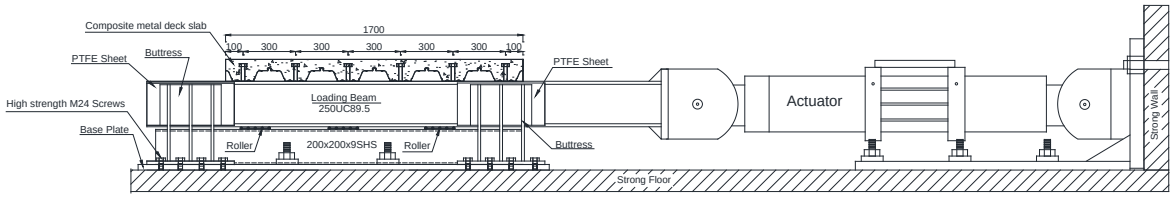

b) Side view

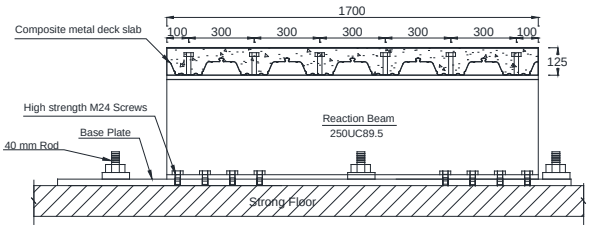

c) Side view

Figure 6. Test rig

2.2 Specimen details

Fig. 7 shows details of the three specimens. As can be seen from Fig. 8, the tested slabs were 1700 mm long in the loading direction, 1160mm wide, 125 mm thick, with 65mm concrete topping on the deck. A total of 18 and 12 headed shear studs were welded to the loading beam and reaction beam respectively and embedded into the concrete slab.

For the first specimen, the rib orientation was parallel to the supporting beams. For the second specimen, the rib orientation was perpendicular to the supporting beams. However, the deck did not continue over the top flange to give a solid concrete rib along the beam. This is the more common edge detail in New Zealand, as it gives a robust slab edge anchorage which is desirable for severe earthquake and severe fire. For the third specimen, the rib orientation was perpendicular to the supporting beams and the deck continued over the top flange.

a) Sp1 b) Sp 2 (New Zealand detail) c) Sp 3 (European detail)

Figure 7. Photograph of specimens

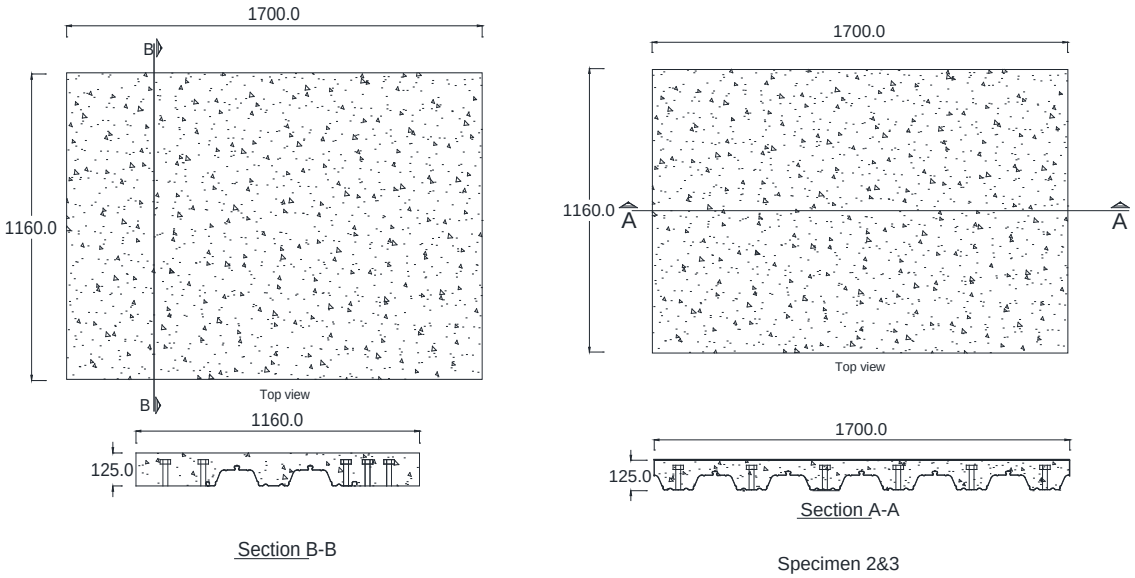

a) Sp 1 configuration (primary spandrel beam) b) Sp 2 & 3 configuration (secondary spandrel beam)

Figure 8. Details of specimens

Fig. 9 shows details of the reinforcing bars. As can be seen, they were arranged such that the probability of failure near the reaction beam was in principle greater than the other regions of the slab. This made it possible to investigate the mechanism of shear load transfer from the slab to the beam. In accordance with New Zealand design provisions, one edge bar (HD12) was placed close to each shear stud and also a DH12 lapped trimmer bar is needed, as considered in the reinforcement design.

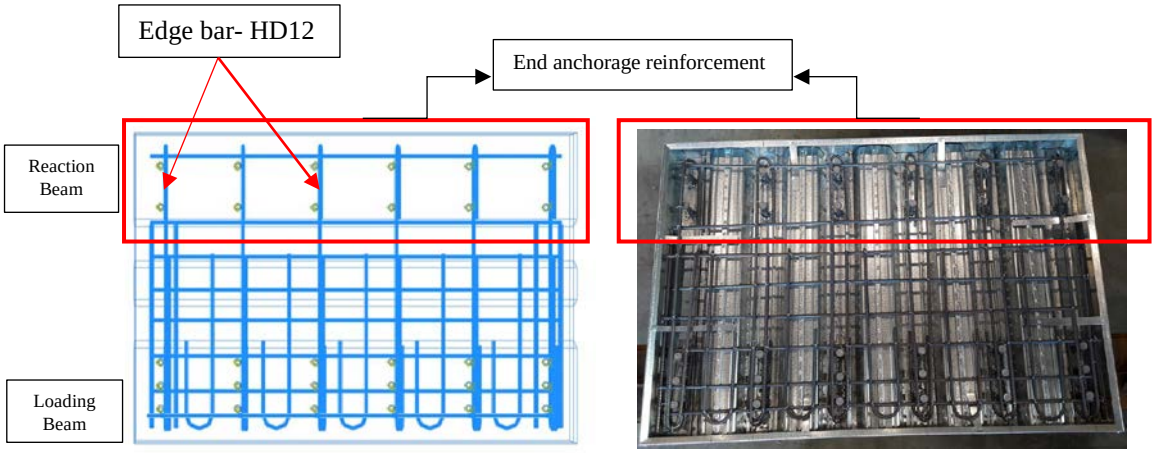

Figure 9. Reinforcement details

2.3 Material properties

2.3.1 Steel deck

Fig. 4 shows the nominal dimensions of the trapezoidal steel decking profile. It has a depth of 60 mm, rib spacing of 300mm and of thickness 0.75mm. The guaranteed minimum yield stress, as specified by the manufacturer is 550 MPa.

2.3.2 Shear connectors

19mm diameter shear studs with 100mm length and a minimum yield strength of 420 MPa were welded to the top flange of steel beams, conforming to the limits set within the international standard ISO 13918:2008.

2.3.3 Reinforcing bars

In accordance with New Zealand design provisions, one DH 12 edge bar with standard hook should be placed close to each shear stud. A DH12 lapped trimmer bar is also needed, and is considered in reinforcement design. Reinforcement was grade 500E to AS/NZS 4671. Eight reinforcing steel tensile tests were performed to determine the material properties of rebars. All samples demonstrated a similar response shown, as shown in Fig. 10.

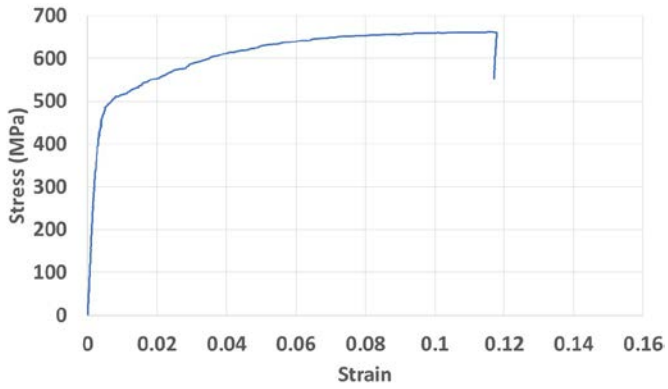

Figure 10. Stress-strain curve for reinforcing bar, with failure occurring outside of the monitored gauge length for deflection, hence the abrupt failure at 12% elongation

2.3.4 Concrete

Cylinder samples were cast and tested to determine the compressive strength of the concrete according to NZS 3112: Part 2:1986. Three samples were taken to determine the compressive strength of 28-day-old concrete cylinders, and, for each specimen, compression testing of three cylinders was conducted within ± 1 day of specimen testing. Concrete samples were subjected to similar curing conditions to the specimens by keeping them in plastic bags and storing each

of the three samples next to a specimen. The mean of the compressive strength of three concrete cylinders for each specimen is reported in Table1.

Table 1. Concrete cylinder strengths (mean of three samples)

Specimen	Age at testing (days)	f_c' (MPa)
	28	29.5
1	125	36
2	145	37.5
3	166	37.5

2.4 Instrumentation and Testing procedure

As shown in Figure 11, each specimen was instrumented with 31 displacement gauges and 10 linear variable displacement transducers (LVDTs) to monitor in-plane displacements, concrete strains, relative slip between the composite slabs and the steel beams at different stages of loading. A data logger system was used to collect all strains and displacements during all the stages of loading. The slabs were tested in force control mode and loading stopped at the steps of 50 kN for crack marking and inspection.

As mentioned previously, the specimens were subjected to a loading rate of 0.01mm/s until failure. After failure occurred, the load continued until it had dropped off to 80% of the ultimate load. High-resolution cameras were used to make videos and take photographs during testing.Load and displacement were continuously monitored and saved at intervals of 0.1 second during testing.

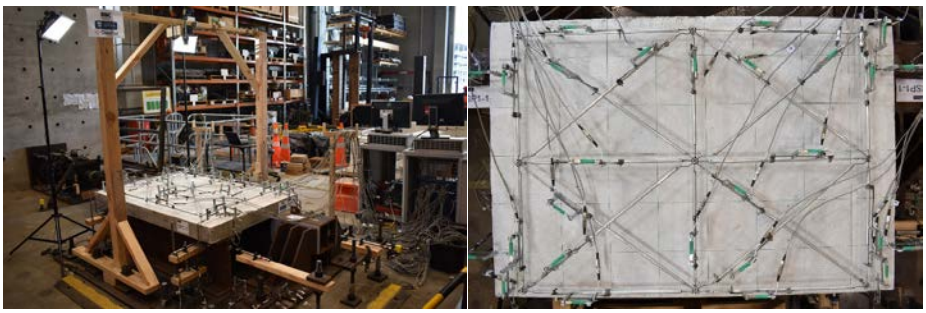

a) General view b) Top view

Figure 11. Instrumentation

3 Results and discussion

3.1 Load-displacement response and strength

Fig. 12 shows the in-plane load-displacement response of the three composite slabs. Table 2 shows the ultimate shear strengths and corresponding displacements. All three specimens exhibited approximately the same ultimate shear strength ($V_{r,exp}$), with specimens 1, 2 and 3 reaching peak loads of 550, 562 and 553 kN respectively. However, these strengths appear at slightly different in-plane displacements of 13.9 mm, 21.7 mm, and 16.6 mm respectively.

As can be seen from Fig. 12, Specimen1 (with the decking parallel to supporting beam) experienced a sharp drop in load carrying capacity and rapid degradation in the post-peak strength, compared to Specimens 2 and 3, which exhibited a more stable and smooth post-peak behaviour, therefore showing superior performance compared to the first specimen.

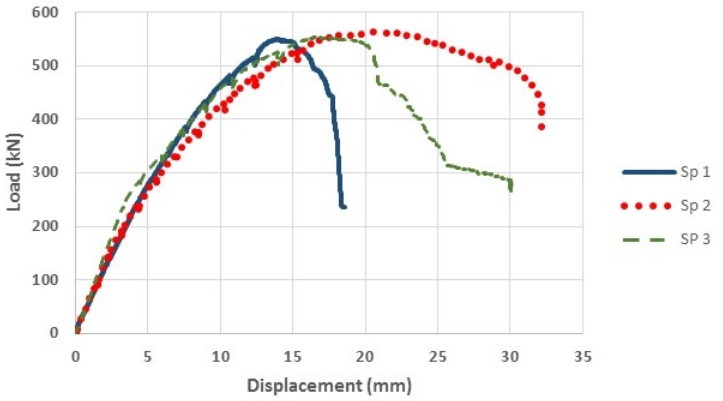

Figure 12. Load-displacement curves

Table 2. Ultimate shear strength and corresponding displacement

Specimen	Ultimate shear strength (kN) $V_{r,exp}$	Displacement at ultimate shear strength Δ_p
	(kN)	(mm)
1	550	13.9
2	562	21.7
3	553	16.6

3.2 Stiffness

The stiffness of a diaphragm system is of paramount importance for seismic design. Degradation of stiffness can adversely affect the response and behaviour of the structures against severe earthquakes and should be considered in the early stages of design. Basically, Diaphragms are designed to behave elastically and remain in the elastic range during severe earthquakes. The elastic stiffness values for all specimens are calculated by the secant stiffness through a point corresponding to 40% of the ultimate shear strength ($V_{r,exp}$).

Diaphragm stiffness was determined at the displacement equal to 1.5 times yield point displacement as well and reported in Table 2. Results revealed that stiffness reduction of three specimens were gradual and even beyond yield point they had considerable stiffness. All easily meet the stiffness requirements from NZS 1170.5 for a rigid diaphragm in the elastic range.

Given that the force-displacement relation may not have a well-defined yield point, the definition of yield displacement exhibits some complexities and several methods have been proposed by researches in the literature [13]. Choosing a suitable method is dependent on the structural behaviour and material properties. The yielding point could be defined based on the test observations and also the load-displacement curve obtained from testing, where the elastic stiffness of specimen changes significantly. Herein yielding point is determined as a point where the diagonal cracks initiated in the specimen which agrees well with the load-displacement curve where its gradient changed obviously, showing the decrease of shear stiffness. Fig. 13 shows load-displacement, yielding point, stiffness and crack propagation at different steps for Sp1. It could be seen that most of cracks propagated over 6th step of loading (250 kN-300 kN) which shows a good agreement with the load-displacement curve where the slop of tangent line (red line), showing elastic shear stiffness (K_e) and the actual load-displacement curve began separating at 280 kN approximately. Consequently, this point could be considered as the yielding point. The corresponding displacement for this load (280kN) is 5.1 mm. As it seen from Fig. 13, the stiffness reduction is quite slow and even for the displacement equal to 1.5 times the yield point displacement; the stiffness lost only less than 25% of its elastic stiffness. In this figure, the slope of green tangent line represents the stiffness at that point. The stiffness reduction percentage for Sp2 and Sp 3 was 35% and 50% respectively. Results for all three specimens are presented in Table 3.

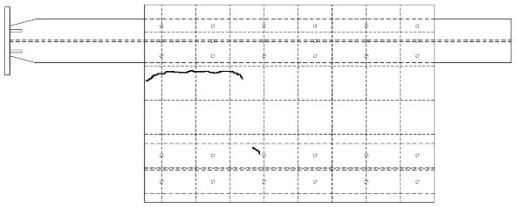

a) Load= 200 kN

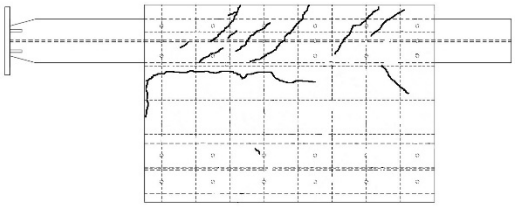

b) Load=250 kN

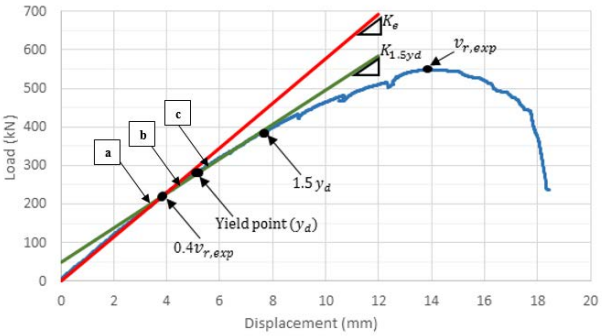

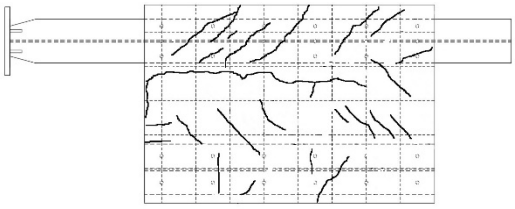

c) Load=300 kN

Figure 13. Stiffness reduction, Sp1

Table 3. Experimental test result

Specimen	Shear elastic stiffness	Stiffness at $1.5y_d$*	Stiffness reduction percentage	Energy dissipation
	(K_e)	$(K_{1.5y_d})$	$\left(K_e - K_{1.5yd} / K_e\right)$	E_d
	(kN/mm)	(kN/mm)	%	(kN.mm)
1	58	44	24	6600
2	58	38	35	13800
3	71	35	50	9300

3.3 Crack patterns and failure modes

The cracking patterns of the three specimens and their sequences were monitored and marked-up during testing on each load step, and are shown in Figs. 14. No cracks formed on

the slabs during the first three steps (50, 100, 150 kN) and the first visible cracks started being generated during the fourth step (150-200 kN) for all specimens. However, due to few cracks with hairline width, no noticeable changes in the strength and stiffness of the slabs could be observed until approximately 300 kN load. Removing formwork (thin steel plates) from outer surfaces revealed that cracks propagated through the depth of the concrete slab.

Two types of cracking pattern were identified due to the specimen configuration. For the first specimen, with parallel ribs to the beams, the main crack generated parallel to and close to the reaction beam, and then expanded when diagonal cracks spread across the slab with particular directions. This main crack occurred over the flute where the slab has the minimum thickness and gradually grew wider during testing. It was 0.1mm wide at the step of 200 kN and reached 0.4mm at the step of 350 kN while few cracks on the loading beam were 0.2mm wide, the rest were hairline cracks (see Fig. 14a).

For the second and third specimens, diagonal cracks spread across the slabs with the distinction that for the second one more cracks concentrated near the loading beam, whereas for the third one more cracks produced around the reaction beam compared to the second specimen. The second specimen experienced its first two cracks during the fourth step of loading (150-200 kN). These cracks were around 0.1mm wide. The crack width became 0.2mm at 350 kN, and increased to 0.5mm at 500 kN (see Fig. 14b).

As with the previous two specimens, the third specimen exhibited its first cracks at a load of 200 kN with width of less than 0.1mm. As loading continued, the length and width of cracks extended and reached 0.3mm, 0.4mm and 0.5mm wide at the loads of 350, 400 and 450 kN respectively. A few cracks increased to 0.7mm at the loading of 550 kN, shortly before failure happened (see Fig. 14c). It is worth noting that no reinforcement or edge bar failure occurred

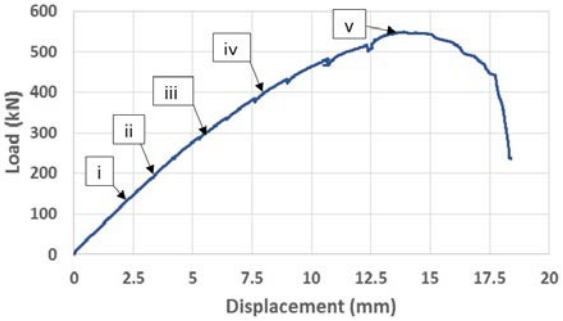

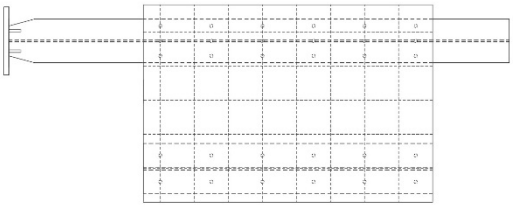

i) Load=150 kN

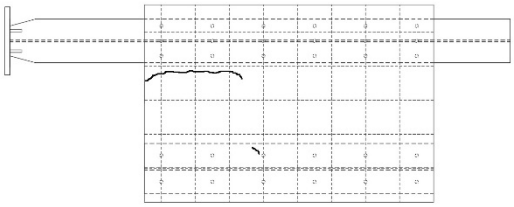

ii) Load=200 kN

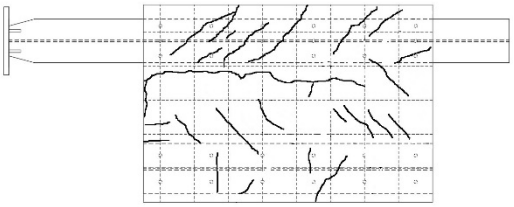

iii) Load=300 kN

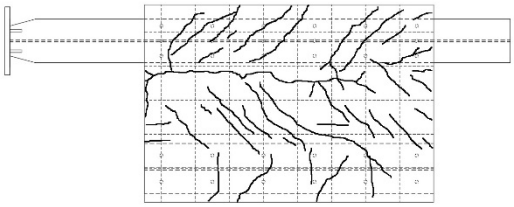

iv) Load=400 kN

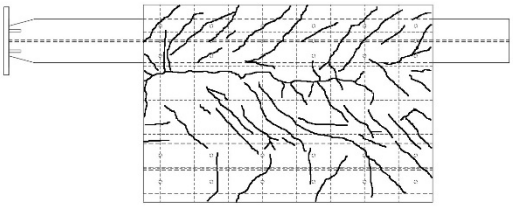

v) Load=550 kN

a) Sp1

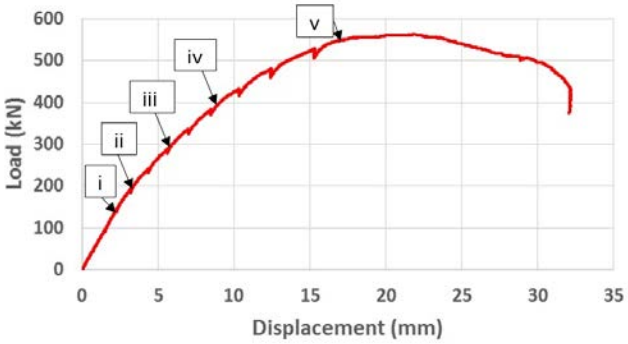

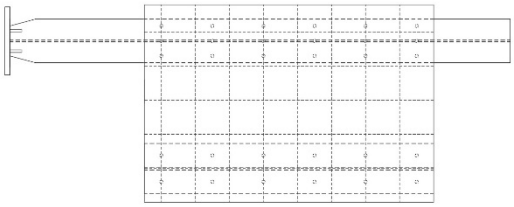

i) Load=150 kN

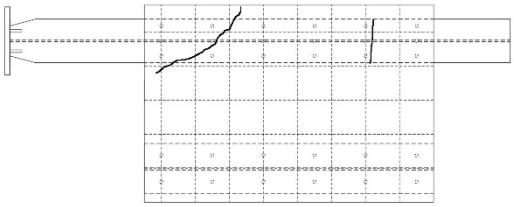

ii) Load=200 kN

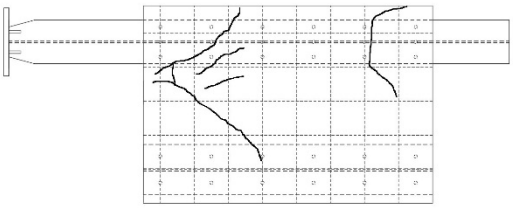

iii) Load=300 kN

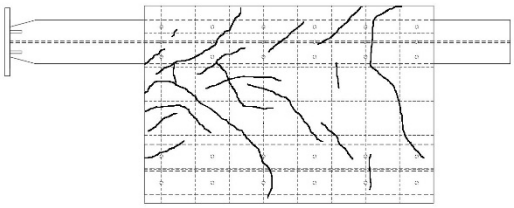

iv) Load=400 kN

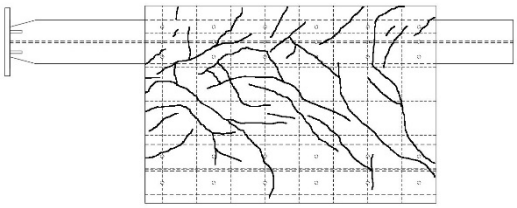

v) Load=550 kN

b) Sp2

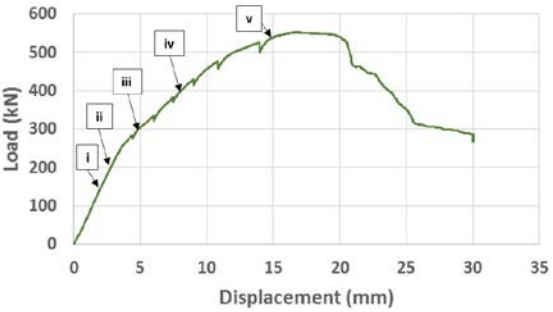

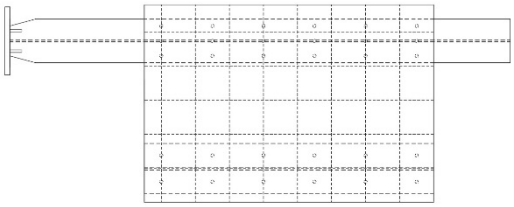

i) Load=150 kN

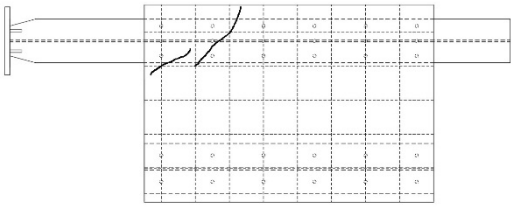

ii) Load=200 kN

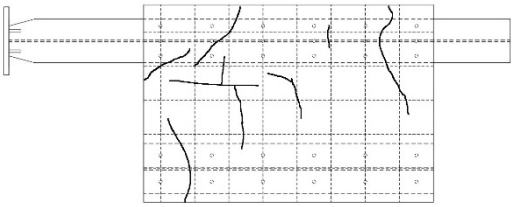

iii) Load=300 kN

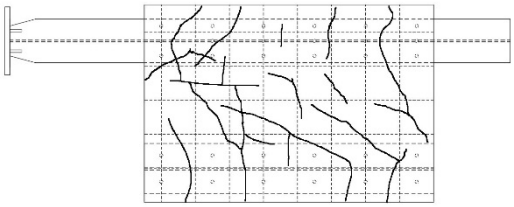

iv) Load=400 kN

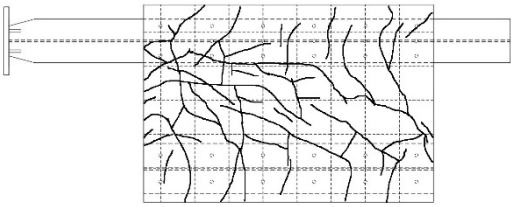

v) Load=550 kN

c) Sp3

Figure 14. Cracking pattern at different stages of loading

For these three composite slabs. Fig. 15 shows failure modes and crack patterns for the three specimens at the last step of loading.

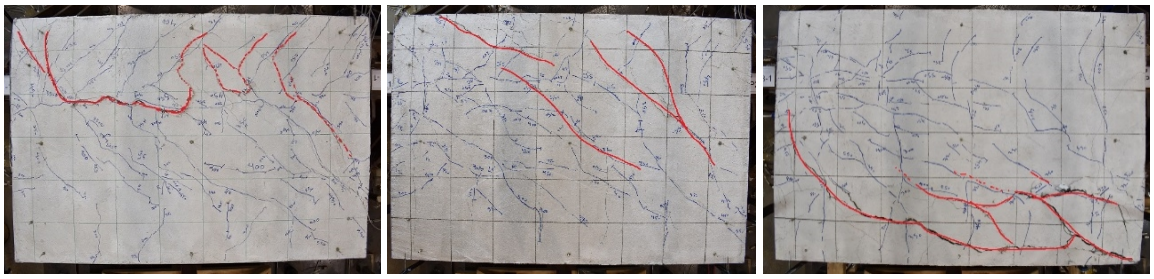

Sp1 Sp2 Sp3

Figure 15. Failure modes and main cracks at the last step

3.4 Slippage of the slab

Fig. 16 shows the position of the displacement gauges. Seven displacement gauges were installed between the steel beams and composite slab at the four corners to measure relative longitudinal and transverse slippage between the composite slab and steel beams.

In a composite slab diaphragm, supported by a steel beam, the composite slab tends to slide along the flange of the beam while shear concertos perform to prevent this slippage; such slippage between adjacent components in a composite member results in a reduction of composite action and is considered as a critical in-plane failure mechanism.

A very small amount of slippage, less than 1mm, was observed between the composite slab and steel beam before failure, and after that, an increased amount of slippage developed. This was likely due to the establishment and development of cracks in the concrete around the base of shear studs, which resulted in loss of concrete compression bulb confining pressure and the stud moving through the crack. It was also observed that there was more slippage at one end of the beam compared to the other end. This could be as a result of initiation of concrete cracking and spalling at that particular end.

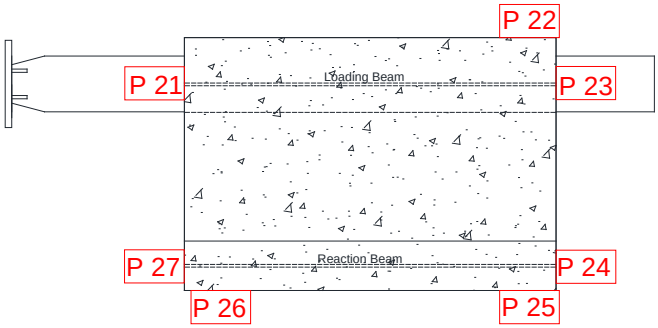

Figure 16. Position of displacement gauges

Fig. 17 presents the development of end slips throughout the loading history for composite slabs (Sp1 and Sp3). The result shows a good agreement with the failure modes where the failure happened on around loading beam for Sp1 while it occurred on the reaction beam for the third specimen, Sp3. Transverse slippages were monitored as well. The maximum measured transverse slippage was around 2mm for both specimens; however, different behaviour was observed between the specimens. For Sp1, maximum transverse slippage was observed on the loading beam, with no noticeable slippage on the reaction beam. However, for Sp3, the amount of slippage was quite similar at three corners and equal to 2mm. These results are also in good alignment with the observed failure modes (see Fig. 18).

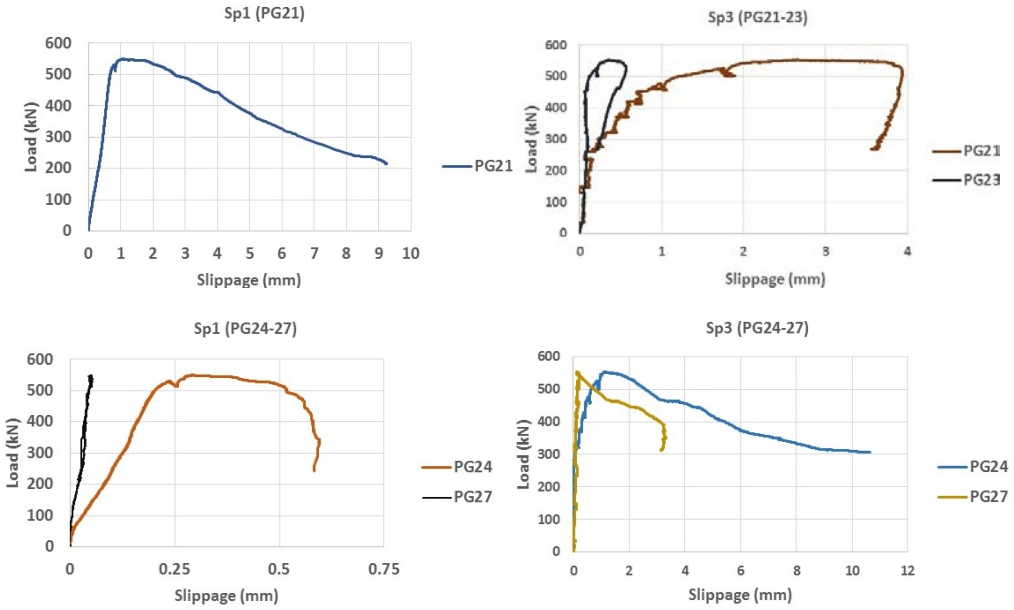

Sp1 Sp3

Figure 17. Longitudinal slippage versus load

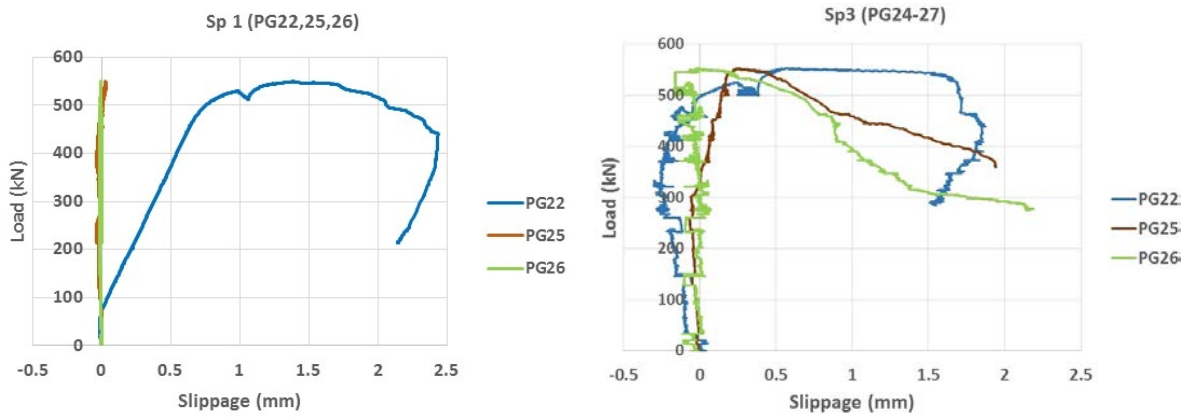

Sp1 Sp3

Figure 18. Transverse slippage versus load

Fig. 19 shows the deformation pattern of a shear stud due to the longitudinal slippage of the slab (Sp3). After concrete removal, inclined shear studs were observed. Heads have displaced 3-7mm, and as a result, slippage between the composite slab and the beam arose. Stud deformation shows a good alignment with the results measured by displacement gauges during testing.

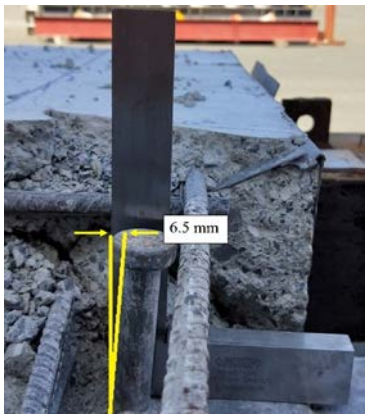

Figure 19. Stud deformation (Sp3)

3.5 Deformation, Buckling and Tearing of decking

Shear force can generate distortion or warping of the profiled steel deck near the ends of the composite slab diaphragm, resulting in interface separation and consequently strength and stiffness degradation. This phenomenon readily occurs in bare steel deck diaphragms and has been well reported by researchers [10, 14, 15]. However, this is a very complicated phenomenon to predict and calculate in composite slabs, due to composite actions between the concrete and steel deck, and it has been less reported and documented for composite slabs in the literature. Once the interface between the deck and concrete breaks down to that extent, the load transfer is lost and the shear-transfer mechanism has been severely compromised [16]. This warping deformation can commonly be seen in composite slabs with the use of arc-spot welds, and is not expected to apply to composite slabs with headed shear studs. However, based on the tests conducted, warping and buckling deformation happened to all specimens at almost the ultimate load (see Fig. 20). The deck punching and tearing of steel deck at connector holes and around the shear studs has been noted by researchers and is considered as one the potential failure modes of composite slabs under in-plane force [17, 18]. This is more likely to be observed in slabs with a single shear stud compared to those with double or triple studs in each rib [19].

Sp1 Sp2 Sp3

Figure 20. Decking deformation

However, tearing of steel deck was observed in Sp2 and Sp3 with multiple shear studs in a rib (see Fig. 21).

Tears in Sp2 were long and easily could be seen from below, while in Sp3 they were quite short and were not visible unless the concert was removed. Fig. 21b shows that punching and tearing of steel sheet happened in front of the stud due to load transferring from the shear stud to the steel deck.

a) Sp2 b) Sp3

Figure 21. Tearing of steel deck

3.6 Energy Dissipation

In a monotonic pushout test, the energy dissipation (E_d) of the specimen is equivalent to the area between the load-displacement curve and displacement axis from the zero to ultimate displacement (Δ_u). The ultimate displacement is defined as the deflection when the load dropped to 80 % of the ultimate load, $V_{r,exp}$ (see Fig. 22). The energy dissipation for three tests are reported in the table 2, indicating that Sp2 had the greatest value among three specimens . The result is consistent with previous research carried out by Matus and Jullien, 2000 [20]. Their study revealed that full concrete slab specimens could dissipate more energy compared to those which have a steel deck. It appears that the solid concrete beam along the top flange of the steel beam played a key role in energy dissipation.

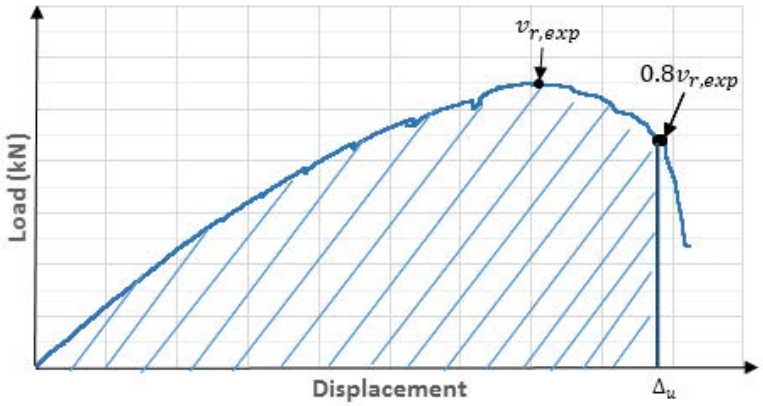

Figure 22. Illustration of energy dissipation

4. Comparison with design standards

Table 4 compares the experimental shear strength against codified equations in the design standards and in the literature. For the North American Standards, an equation by Easterling and Porter [21] is used, based on the ACI shear wall equation:

$$V_r = 3.2(\, t_c + n_s\, t \left(\frac{p}{p'}\right))\, b\, \sqrt{f_c'} \qquad (1)$$

As can be seen from Table 4, the experimentally recorded ultimate shear strength of all three specimens were similar. However, both AS/NZS 2327:2017[22] and EN 1994-1-1:2004 [23] predict a much higher shear strength for Sp3 which uses the European detail. This revealed that contribution of the steel deck and shear studs to the diaphragm interface shear capacity is negligible, compared with the significant contribution predicted by these equations.

Also, the same two standards i.e. AS/NZS 2327:2017 and EN 1994-1-1:2004 predict the same ultimate shear strength for Sp1 and Sp2. This is because only the thickness of the concrete above steel desk is considered to calculate the area of concrete in shear planes.

Also NZ 3404:1997 [24] predicted values for Sp1 and Sp2 are overestimate. A modification to NZ 3404:1997 was proposed by Cowie et al to allow it to cover Sp3. This is by adding the influence of the steel deck, but it can be seen that this officiation has over predicted the strength of Sp3 by a factor of 3.

The Easterling and Porter equation considers the influence of the steel deck by converting the steel thickness to an equivalent concrete thickness. However, it leads to a conservative predicting for the ultimate shear strength. The equation does not include the influence of the edge rebar, which all the other equations have done. The authors have proposed that by adding on the influence of the edge rebars a better prediction can be obtained.

$$V_r = 3.2(\, t_c + n_s\, t \left(\frac{p}{p'}\right))\, b \sqrt{f_c'} \;+\; A_{rt} f_{yr} \qquad (2)$$

It should be mentioned that all strength reduction and capacity factors in the above equations were taken as one and actual tested material properties have been taken in order to determine the calculated actual ultimate shear strength of diaphragms. Fig 23 compares results from the test and mentioned codes above. Dotted line represents the yield point. As it could be seen, design shear strengths from AS/NZS 2327:2017 and EN 1994-1-1:2004 are quite close to the yield point that indicates the diaphragm remain elastic if it is well designed and constructed in accordance to those Standards.

Table 4. Ultimate shear strength of specimens

Specimen	Experimental	Rezeaian et al	Calculated diaphragm interface capacity from existing design equations (kN)				
			Easterling and Porter	EN 1994-1-1:2004	AS/NZS 2327:2017	NZ 3404:1997	Cowie et al
	(kN)	(kN)					
1	550	527	188	337	424	576	-
2	562	608	269	337	424	717	-
3	553	608	269	1072	751	-	1490

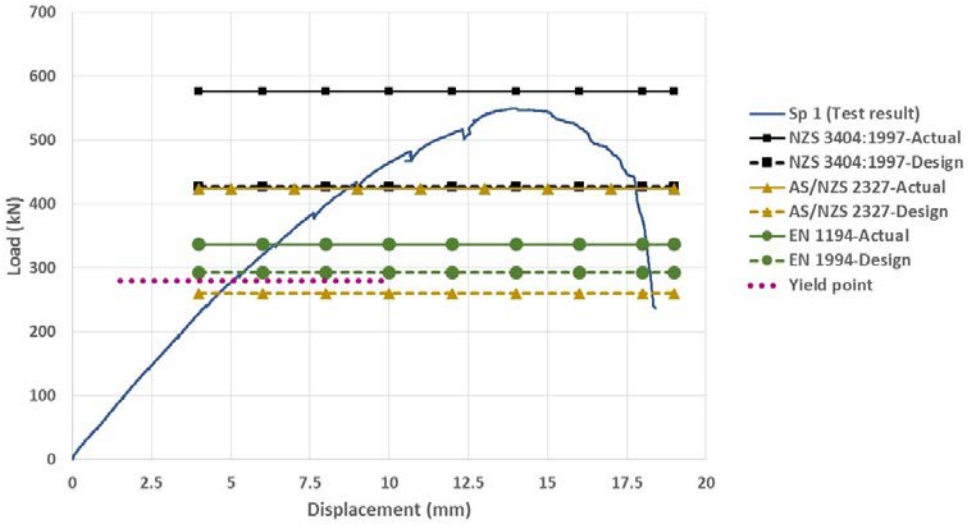

a)

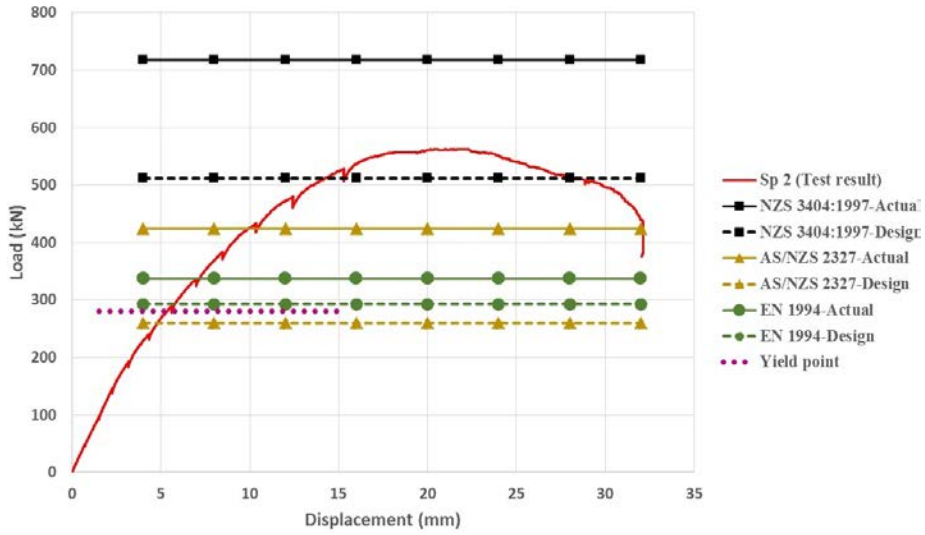

b)

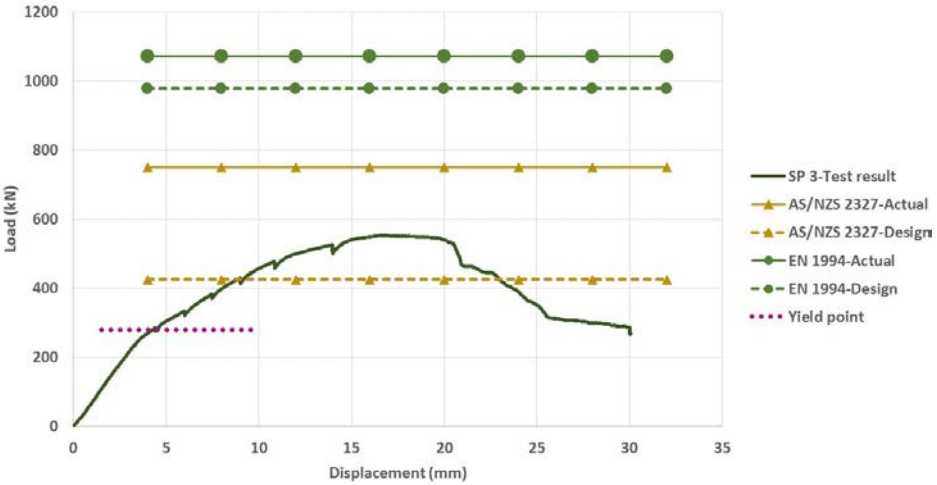

c)

Figure 23. Test results and codified equations a) Sp1, b) Sp2, c) Sp3

5 CONCLUSIONS

In this paper, the in-plane shear behaviour of composite slabs with three different configurations of decking was examined through monotonic tests. These tests included specimens with ribs that had an orientation either parallel (Sp1) or perpendicular (Sp2 & Sp3) to the reaction beam. For Sp2, steel decking didn't continue over the top flange of the reaction beam, whereas it continued in Sp3. For Sp1 and Sp2, the shear studs were not welded through the decking, with the decking pinned to the beam. For Sp3, the shear studs were welded to the beam through decking. Load-displacement and slippage were measured, the cracking patterns were mapped through diffident stages of loading, and the failure modes were reported as well. Key findings and conclusions are summarised as follows:

- Monotonic tests on the three different diaphragm interface configurations show very similar strength and stiffness in the elastic range despite predictions of diaphragm strength giving significantly different strengths.
- The peak shear strength reached in all three specimens was close (around 555 kN) although it happened at slightly different displacements.
- The first specimen (Sp1, Ribs parallel to the supporting beam) experienced a significant drop in load carrying capacity and rapid degradation in the post-peak strength compared to the 2nd and 3rd specimens (Sp2 & Sp3, ribs orientation perpendicular to the supporting beam) there was little difference in peak load between Sp2 and Sp3, with the latter being more ductile.
- The modes of failure were different to those predicted by the current design equations, and so new mechanisms and associated equations have had to be developed.
- Reinforcement or shear stud (shank or welding) fracture did not occur in any of these three specimens.
- The reduction of stiffness in all three specimens up to peak load was slight.
- Buckling and deformation of the steel deck occurred in all three specimens before the ultimate load. Punching and tearing of the steel deck could be seen at a few points of steel deck adjacent to the shear stud. Two long tears of the steel decking were observed in the second specimen.
- Very similar peak strengths ($v_{r,exp}$) of Sp2 and Sp3 show that the through deck welded shear studs have no influence on the peak strength of the diaphragm interface, although they do slightly increase the stiffness in the elastic range.

- AS/NZS 2327 and EN 1994-1-1:2004 give a reliable design strength for Sp1 and Sp2. However, these Standards significantly overestimate the design shear strength for Sp3. Based on the test result contribution of steel deck and shear studs in shear strength of composite diaphragm is negligible.

ACKNOWLEDGEMENTS

The authors would like to thank The Earthquake Commission (EQC) for funding this research project. The steel decking and shear studs were provided by ComFlor, which is gratefully acknowledged. The authors would also like to acknowledge the support received from all the technical staff at The University of Auckland. This support is much appreciated.

RERERENCES

1. Crisinel, M. and D. O'Leary, *Composite floor slab design and construction.* Structural engineering international, 1996. **6**(1): p. 41-46.
2. Sangeetha, M.R., et al., *State of Art on Composite Slab Construction.* International Journal of Applied Environmental Sciences, 2018. **13**(1): p. 1-8.
3. Fleischman, R.B. and K.T. Farrow, *Dynamic behavior of perimeter lateral-system structures with flexible diaphragms.* Earthquake Engineering and Structural Dynamics, 2001. **30**(5): p. 745-763.
4. Rodriguez, M.E., J.I. Restrepo, and J.J. Blandón, *Seismic design forces for rigid floor diaphragms in precast concrete building structures.* Journal of structural engineering, 2007. **133**(11): p. 1604-1615.
5. Samuel Easterling, W. and C.S. Young, *Strength of composite slabs.* Journal of Structural Engineering, 1992. **118**(9): p. 2370-2389.
6. Abdullah, R. and W.S. Easterling, *Determination of composite slab strength using a new elemental test method.* Journal of Structural Engineering, 2007. **133**(9): p. 1268-1277.
7. Lopes, E. and R. Simoes, *Experimental and analytical behaviour of composite slabs.* Steel and Composite Structures, 2008. **8**(5): p. 361-388.
8. Hedaoo, N.A., L.M. Gupta, and G.N. Ronghe, *Design of composite slabs with profiled steel decking: a comparison between experimental and analytical studies.* International Journal of Advanced Structural Engineering, 2012. **4**(1): p. 1.
9. Altoubat, S., H. Ousmane, and S. Barakat, *Experimental Study of In-Plane Shear Behavior of Fiber-Reinforced Concrete Composite Slabs.* Journal of Structural Engineering, 2016. **142**(3): p. 04015156.
10. Luttrell, L.D. and G. Winter, *Structural performance of light gage steel diaphragms.* 1965.
11. Davies, J. and J. Fisher, *THE DIAPHRAGM ACTION OF COMPOSITE SLABS.* Proceedings of the Institution of Civil Engineers, 1979. **67**(4): p. 891-906.
12. AS/NZS1252, *High-strength steel fastener assemblies for structural engineering - Bolts, nuts and washers*. 2016, Standards Australia and Standards New Zealand: Sydney, Australia and Wellington, New Zealand.

13. Park, R. *Ductility evaluation from laboratory and analytical testing*. in *Proceedings of the 9th world conference on earthquake engineering, Tokyo-Kyoto, Japan*. 1988.
14. Luttrell, L.D., *Steel Deck Institute diaphragm design manual.* 2006.
15. Avci, O., et al., *Diaphragm shear strength and stiffness of aluminum roof panel assemblies.* Thin-Walled Structures, 2016. **106**: p. 51-60.
16. Easterling, W.S. and M.L. Porter, *Steel-deck-reinforced concrete diaphragms. I.* Journal of Structural Engineering, 1994. **120**(2): p. 560-576.
17. Prins, M.D., *Elemental tests for the seismic resistance of composite floor diaphragms*. 1985, IOWA State University.
18. Qureshi, J., D. Lam, and J. Ye, *The influence of profiled sheeting thickness and shear connector's position on strength and ductility of headed shear connector.* Engineering Structures, 2011. **33**(5): p. 1643-1656.
19. Rehman, N., et al., *Experimental study on demountable shear connectors in composite slabs with profiled decking.* Journal of Constructional Steel Research, 2016. **122**: p. 178-189.
20. Matus, R.A. and J.F. Jullien. *A High Seismic Performance Shear Connector for Composite Steel-Concrete Structures Subjected to Strong Earthquakes*. in *Composite Construction in Steel and Concrete IV*. 2000. Alberta, Canada.
21. Easterling, W. and M. Porter, *Behavior, analysis and design of steel-deck-reinforced concrete diaphragms*, in *Final Report, Project*. 1988: Ames, IA, USA.
22. *AS/NZS 2327, Composite structures-Composite steel-concrete construction in buildings*, in *Australian/New Zealand Standard*. 2017: Sydney, Australia.
23. 305/2011, T.E.U.P.R., *EN 1994-1-1 (2004): Eurocode 4* in *Design of composite steel and concrete structures – Part 1-1: General rules and rules for buildings* 2004.
24. *NZS 3404: 1997, Steel Structures Standard*, in *Standards New Zealand, Wellington*. 2007.